Nigerian Journal of Physics (NJP)
ISSN online: 3027-0936
ISSN print: 1595-0611
DOI: https://doi.org/10.62292/njp.v35i1.2026.477
Volume 35(1), March 2026

Magnetic Properties of Titanium Hydride (TiH) Diatomic Molecule with Modified Kratzer Energy-Dependent Screened Coulomb Potential in the Presence of Magnetic and Aharonov-Bohm Flux Fields

***[1]Ishaya Sunday Danladi, [2]Yakubu Yerima Jabil and [2]Lawrence Davou Christopher**

[1]NNPC Downstream Investment Service, NNPC Towers, Central Business District Abuja, Abuja, Nigeria.
[2]Department of Physics, University of Jos, Plateau State, Nigeria.

*Corresponding Author's Email: ishayadan@gmail.com

ABSTRACT

In this study, the modified Kratzer energy-dependent screened Coulomb potential is analyzed in the presence of external magnetic and Aharonov–Bohm (AB) flux fields. The Schrödinger equation is solved using the Nikiforov–Uvarov Functional Analysis (NUFA) method, yielding closed-form expressions for the energy eigenvalues and the corresponding wavefunctions. These solutions are applied to investigate the magnetic properties of the titanium hydride (TiH) diatomic molecule, including the partition function, magnetization, magnetic susceptibility, and persistent current. The effects of the slope parameter are examined in detail and found to play a significant role in controlling the magnitude, ordering, and convergence behavior of all magnetic observables. Negative slope values enhance the magnetic and thermodynamic responses of the system, while positive slope values suppress them, with the zero-slope case acting as an intermediate regime. The magnetic field induces divergence and saturation effects, whereas the AB-flux field governs sharp transitions, minima, and convergence characteristics. Overall, the results demonstrate that both the slope parameter and external fields provide effective mechanisms for tuning the magnetic behavior of the TiH diatomic molecule.

Keywords:
Aharonov–Bohm (AB) flux,
Magnetic properties,
Slope parameter,
Titanium Hydride (TiH) Diatomic molecule.

INTRODUCTION

In fact, the study of diatomic molecules (DMs) is a crucial aspect of quantum chemistry and atomic physics. Several authors have recently examined the solution of relativistic and nonrelativistic wave equations to understand the behaviours of numerous DMs in various molecular potentials (Abu-Shady, Abdel-Karim & Khokha, 2021).

The analytical solution of the radial Schrodinger Equation (SE) is of high importance in nonrelativistic quantum mechanics, since the wave function contains all the necessary information to describe a quantum system fully.

Recent studies have incorporated the thermodynamic properties of these systems to better understand their behavior. For instance (Gumber, Kumar, Gambhir, Mohan & Kumar, 2015) investigated the properties of a two-dimensional cylindrical quantum dot in the presence of both electric and magnetic fields, calculating the canonical partition function along with other statistical mechanical properties. The partition function, a key quantity in statistical mechanics, is used to evaluate thermal properties, with its temperature dependence allowing for the computation of thermodynamic variables such as heat capacity, entropy, and free energy. The concept of the partition function, introduced by Boltzmann in the 1870s (Ebeling & Sokolov, 2005), plays a central role in these analyses. Eshghi, Mehraban & Ikhdair (2017) also obtained energy eigenvalues and examined the thermal properties of a position-dependent mass charged particle influenced by external magnetic fields. Oyewumi *et al*. (2014) studied the radial Schrödinger equation with a Deng–Fan potential model, calculating the system's thermodynamic properties and analyzing how the partition function, heat capacity, entropy, mean energy, and free energy varied with temperature. Using the Pseudoharmonic potential in the presence of both magnetic and AB fields, Ikot *et al*. (2020) investigated thermodynamic properties within the framework of superstatistics. Song, Wang & Jia (2017) computed the thermodynamic properties of a sodium dimer under the improved Rosen–Morse potential, finding good agreement with experimental results. Dong

and Cruz-Irisson (2012) analyzed the thermodynamic properties of the modified Rosen-Morse potential using an appropriate quantization rule. Onate & Onyeaju (2016) calculated the thermodynamic properties of the Frost-Musulin potential via partition function, while Ikot *et al*. (2019) studied the exact and Poisson summation thermodynamic properties for diatomic molecules with Tietz potential. Further, Ikot *et al*. (2020) explored the screened Kratzer potential in the presence of both magnetic and AB flux fields in two-dimensional space, using the factorization method and investigating a range of thermodynamic properties. Ikot *et al*. (2019) demonstrated that by solving the Schrödinger equation for the screened Kratzer potential, one can derive the vibrational partition function and subsequently compute various thermodynamic properties of diatomic systems.
Extending these approaches to systems under external influences, Edet *et al*. (2021) showed that the inclusion of magnetic and Aharonov–Bohm fields in a Yukawa potential framework results in discernible shifts in energy eigenvalues that directly affect persistent currents, magnetic susceptibility, and related thermal properties. Nevertheless, despite the extensive body of existing research, our review reveals that the magnetic properties of the titanium hydride (TiH) diatomic molecule, modeled using the modified Kratzer energy-dependent screened Coulomb potential, have not yet been investigated in the presence of external magnetic and Aharonov–Bohm (AB) flux fields. Addressing this gap constitutes the primary objective of the present study. The modified Kratzer energy-dependent screened Coulomb potential is given by:

$$V(r,E_{nm}) = D_e\left(\frac{r-r_e}{r}\right)^2 - \frac{C}{r}(1+\tilde{\mathrm{g}}E_{nm})e^{-\delta \mathrm{r}} \qquad (1)$$

where D_e is the dissociation energy, r_e is the equilibrium internuclear separation, C is the depth of the potential, δ is the screening parameter, and $\tilde{\mathrm{g}}$ is the slope parameter and can be adjusted as desired.

MATERIALS AND METHODS

In this section, we briefly introduce the Nikiforov-Uvarov Functional Analysis (NUFA) method (Ikot *et. al.,* 2021). This method is useful to solve second-order differential wave equations of the hypergeometric-type:

$$\frac{d^2\psi(s)}{ds^2} + \frac{\tilde{\tau}(s)}{\sigma(s)}\frac{d\psi(s)}{ds} + \frac{\tilde{\sigma}(s)}{\sigma^2(s)}\psi(s) = 0 \qquad (2)$$

where $\sigma(s)$ and $\tilde{\sigma}(s)$ are polynomials at most second degree, and $\tilde{\tau}(s)$,is a first degree polynomial. Tezcan and Sever (2008), latter introduced the parametric form of NU method in the form

$$\frac{d^2\psi(s)}{ds^2} + \frac{\alpha_1-\alpha_2 s}{s(1-\alpha_3 s)}\frac{d\psi(s)}{ds} + \frac{1}{s^2(1-\alpha_3 s)^2}[-\xi_1 s^2 + \xi_2 s - \xi_3]\psi(s) = 0 \qquad (3)$$

where α_i and $\xi_i (i = 1,2,3)$ are all parameters. It can be observed in Eq. (3) that the differential equation has two singularities at $s \to 0$ and $s \to 1$, thus it takes the wave function in the form

$$\psi(s) = s^{\lambda}(1-s)^{v} f(s) \qquad (4)$$

Substituting Eq. (4) into Eq. (3) leads to the following equation

$$s(1-\alpha_3 s)\frac{d^2f(s)}{ds^2} + [\sigma_1 + 2\lambda - (2\lambda\alpha_3 + 2v\alpha_3 + \alpha_2)s]\frac{df(s)}{ds} - \alpha_3\left(\lambda + v + \frac{1}{2}\left(\frac{\alpha_2}{\alpha_3}-1\right) + \sqrt{\frac{1}{4}\left(\frac{\alpha_2}{\alpha_3}-1\right)^2 + \frac{\xi_1}{\alpha_3^2}}\right)\left(\lambda + v + \frac{1}{2}\left(\frac{\alpha_2}{\alpha_3}-1\right) - \sqrt{\frac{1}{4}\left(\frac{\alpha_2}{\alpha_3}-1\right)^2 + \frac{\xi_1}{\alpha_3^2}}\right) + \left[\frac{\lambda(\lambda-1)+\alpha_1\lambda-\xi_3}{s} + \frac{v(v-1)\alpha_3+\alpha_2 v-\alpha_1\alpha_3 v-\frac{\xi_1}{\alpha_3}+\xi_2-\xi_3\alpha_3}{(1-\alpha_3 s)}\right]f(s) = 0 \qquad (5)$$

Eq. (5) can be reduced to a Gauss hypergeometric equation if and only if the following functions vanish

$$\lambda(\lambda-1) + \alpha_1\lambda - \xi_3 = 0 \qquad (6)$$

$$v(v-1)\alpha_3 + \alpha_2 v - \alpha_1\alpha_3 v - \frac{\xi_1}{\alpha_3} + \xi_2 - \xi_3\alpha_3 = 0 \qquad (7)$$

Thus, Eq. (5) now becomes

$$s(1-\alpha_3 s)\frac{d^2f(s)}{ds^2} + [\sigma_1 + 2\lambda - (2\lambda\alpha_3 + 2v\alpha_3 + \alpha_2)s]\frac{df(s)}{ds} - \alpha_3\left(\lambda + v + \frac{1}{2}\left(\frac{\alpha_2}{\alpha_3}-1\right) + \sqrt{\frac{1}{4}\left(\frac{\alpha_2}{\alpha_3}-1\right)^2 + \frac{\xi_1}{\alpha_3^2}}\right)\times \left(\lambda + v + \frac{1}{2}\left(\frac{\alpha_2}{\alpha_3}-1\right) - \sqrt{\frac{1}{4}\left(\frac{\alpha_2}{\alpha_3}-1\right)^2 + \frac{\xi_1}{\alpha_3^2}}\right)f(s) = 0 \qquad (8)$$

Solving Eqs. (6) and (7) completely give

$$\lambda = \frac{1}{2}\left((1-\alpha_1) \pm \sqrt{(1-\alpha_1)^2 + 4\xi_3}\right) \qquad (9)$$

$$v = \frac{1}{2\alpha_3}\left((\alpha_3 + \alpha_1\alpha_3 - \alpha_2) \pm \sqrt{(\alpha_3 + \alpha_1\alpha_3 - \alpha_2)^2 + 4\left(\frac{\xi_1}{\alpha_3} + \alpha_3\xi_3 - \xi_2\right)}\right) \qquad (10)$$

Eq. (8) is the hypergeometric equation type of the form

$$x(1-x)\frac{d^2f(x)}{dx^2} + [c + (a+b+1)x]\frac{df(x)}{dx} - [ab]f(x) = 0 \qquad (11)$$

where a, b, and$c$ are given as follows

$$a = \sqrt{\alpha_3}\left(\lambda + v + \frac{1}{2}\left(\frac{\alpha_2}{\alpha_3} - 1\right) + \sqrt{\frac{1}{4}\left(\frac{\alpha_2}{\alpha_3} - 1\right)^2 + \frac{\xi_1}{\alpha_3^2}}\right) \quad (12)$$

$$b = \sqrt{\alpha_3}\left(\lambda + v + \frac{1}{2}\left(\frac{\alpha_2}{\alpha_3} - 1\right) - \sqrt{\frac{1}{4}\left(\frac{\alpha_2}{\alpha_3} - 1\right)^2 + \frac{\xi_1}{\alpha_3^2}}\right) \quad (13)$$

$$c = \alpha_1 + 2\lambda \quad (14)$$

Setting either $a$or b equal to a negative integer$-n$, the hypergeometric function $f(s)$ turns to a polynomial of degree n. Hence, the hypergeometric function $f(s)$ approaches finite in the following quantum condition i.e. $a = -n$, where $n = 0,1,2,3,\ldots..n_{max}$

Using the above quantum condition,

$$\sqrt{\alpha_3}\left(\lambda + v + \frac{1}{2}\left(\frac{\alpha_2}{\alpha_3} - 1\right) + \sqrt{\frac{1}{4}\left(\frac{\alpha_2}{\alpha_3} - 1\right)^2 + \frac{\xi_1}{\alpha_3^2}}\right) = -n \quad (15)$$

$$\lambda + v + \frac{1}{2}\left(\frac{\alpha_2}{\alpha_3} - 1\right) + \frac{n}{\sqrt{\alpha_3}} = -\sqrt{\frac{1}{4}\left(\frac{\alpha_2}{\alpha_3} - 1\right)^2 + \frac{\xi_1}{\alpha_3^2}} \quad (16)$$

Squaring both sides of Eq. (16) and rearranging, one obtains the energy equation for the NUFA method as

$$\lambda^2 + 2\lambda\left(v + \frac{1}{2}\left(\frac{\alpha_2}{\alpha_3} - 1\right) + \frac{n}{\sqrt{\alpha_3}}\right) + \left(v + \frac{1}{2}\left(\frac{\alpha_2}{\alpha_3} - 1\right) + \frac{n}{\sqrt{\alpha_3}}\right)^2 - \frac{1}{4}\left(\frac{\alpha_2}{\alpha_3} - 1\right)^2 - \frac{\xi_1}{\alpha_3^2} = 0 \quad (17)$$

By substituting Eqs. (9) and (10) into Eq. (4), one obtains the corresponding wave equation for the NUFA method as

$$\psi(s) = \mathbb{N}s^{\frac{(1-\alpha_1)+\sqrt{(\alpha_1-1)^2+4\xi_3}}{2}}(1-\alpha_3 s)^{\frac{(\alpha_3+\alpha_1\alpha_3-\alpha_2)+\sqrt{(\alpha_3+\alpha_1\alpha_3-\alpha_2)^2+4\left(\frac{\xi_1}{\alpha_3}+\alpha_3\xi_3-\xi_2\right)}}{2\alpha_3}}{}_2F_1(a,b,c;s) \quad (18)$$

where $\mathbb{N}$ is the normalization constant.

Only the positive sign is used above because it ensures a normalizable, physically acceptable wavefunction and produces discrete bound-state energies, while the negative sign leads to divergent or non-physical solutions.

Solution of the 2D Schrodinger Equation TiH Diatomic Molecule with Magnetic and AB-flux Fields

A generalized form of the Schrodinger Equation (SE) for a charged particle moving under the influence of the vector potential $\vec{A}$ is written as (Purohit *et al*., 2020; Rampho *et al*., 2020; Ikot *et al*., 2020):

$$\left(i\hbar\vec{\nabla} + \frac{e}{c}\vec{A}\right)^2 \psi(r,\phi) = 2\mu[E_{nm} - V(r)]\psi(r,\phi) \quad (19)$$

where e and μ are the charge of the particle and reduced mass of the system, respectively, E_{nm} is the energy eigenvalues, $c$is the velocity of light, $\vec{A}$ is the vector potential and $V(r)$ scalar potential. To indicate the magnetic field and AB-flux field together, we express the vector potential $\vec{A}$ as a sum of two terms $\vec{A} = \vec{A}_1 + \vec{A}_2$having azimuthal components

$$\vec{A}_1 = \frac{\vec{B}e^{-\delta r}}{1-e^{-\delta r}}\hat{\phi} \text{ and } \vec{A}_2 = \frac{\Phi_{AB}}{2\pi r}\hat{\phi} \quad (20)$$

where $\vec{B}$ is the applied external magnetic field with $\vec{\nabla} \times \vec{A}_1 = \vec{B}, \vec{A}_2$represents the additional magnetic flux $\Phi_{AB} = \xi$ created by a solenoid with $\vec{\nabla} \cdot \vec{A}_2 = 0$. Then the vector potential $\vec{A}$ can be written as:

$$\vec{A} = \left(\frac{\vec{B}e^{-\delta r}}{1-e^{-\delta r}} + \frac{\xi}{2\pi r}\right)\hat{\phi} \quad (21)$$

where $\hat{\phi}$ is the direction of magnetic flux around the solenoid. Also, we assume a wavefunction in the cylindrical coordinates to be of the form:

$$\psi(r,\phi) = (2\pi r)^{-\frac{1}{2}}e^{im\phi}\Omega_{nm}(r) \quad (22)$$

where m is the magnetic quantum number.

Substituting Eq. (1) into Eq. (19), we have

$$\left(i\hbar\vec{\nabla} + \frac{e}{c}\vec{A}\right)^2 \psi(r,\phi) = 2\mu\left[E_{nm} - D_e\left(\frac{r-r_e}{r}\right)^2 + \frac{C}{r}(1+\tilde{g}E_{nm})e^{-\delta r}\right]\psi(r,\phi) \quad (23)$$

For convenience, let us introduce $\lambda = \frac{e}{c}$, so that Eq. (23) becomes

$$\left(i\hbar\vec{\nabla} + \lambda\vec{A}\right)^2\psi(r,\phi) = 2\mu\left[E_{nm} - D_e + \frac{2D_e r_e}{r} - \frac{D_e r_e^2}{r^2} + \frac{C}{r}e^{-\delta r} + \frac{C\tilde{g}E_{nm}}{r}e^{-\delta r}\right]\psi(r,\phi) \quad (24)$$

Using Eqs. (21) and (22) into Eq. (24) we get the 2nd order differential equation (DE) given as follows:

$$\Omega_{nm}^{''}(r)+\left[\begin{matrix}\frac{2\mu}{\hbar^2}\left(E_{nm}-D_e+\frac{2D_er_e}{r}-\frac{D_er_e^2}{r^2}+\frac{C}{r}e^{-\delta r}+\frac{C\tilde{g}E_{nm}}{r}e^{-\delta r}\right)+\frac{1}{4r^2}-\frac{m^2}{r^2}\\+\frac{2m\lambda\vec{B}e^{-\delta r}}{\hbar(1-e^{-\delta r})r}+\frac{m\lambda\xi}{\hbar\pi r^2}-\frac{\lambda^2\vec{B}^2e^{-2\delta r}}{\hbar^2(1-e^{-\delta r})^2}-\frac{\lambda^2\vec{B}\xi e^{-\delta r}}{\hbar^2(1-e^{-\delta r})\pi r}-\frac{\lambda^2\xi^2}{4\pi^2\hbar^2r^2}\end{matrix}\right]\Omega_{nm}(r)=0 \quad (25)$$

Equation (25) is a complicated differential equation that cannot be solved easily due to the presence of centrifugal $\frac{1}{r^2}$ as well as the reciprocal $\frac{1}{r}$ terms. Therefore, to bypass these terms we introduce the Greene-Aldrich approximation scheme (Greene & Aldrich, 1976). These approximations are given by:

$$\frac{1}{r^2}\approx\frac{\delta^2}{(1-e^{-\delta r})^2}\text{ and }\frac{1}{r}\approx\frac{\delta}{(1-e^{-\delta r})} \quad (26)$$

Using the approximation terms of Eqs. (26) into Eq. (25) we have:

$$\Omega_{nm}^{''}(r)+\left[\begin{matrix}\frac{2\mu E_{nm}}{\hbar^2}-\frac{2\mu D_e}{\hbar^2}+\frac{4\mu\delta D_er_e}{\hbar^2(1-e^{-\delta r})}-\frac{2\mu\delta^2D_er_e^2}{\hbar^2(1-e^{-\delta r})^2}\\+\frac{2\mu\delta C}{\hbar^2(1-e^{-\delta r})}e^{-\delta r}+\frac{2\mu\delta C\tilde{g}E_{nm}}{\hbar^2(1-e^{-\delta r})}e^{-\delta r}+\frac{2m\delta\lambda\vec{B}}{\hbar(1-e^{-\delta r})^2}e^{-\delta r}\\-\frac{\lambda^2\vec{B}^2}{\hbar^2(1-e^{-\delta r})^2}e^{-2\delta r}-\frac{\lambda^2\delta\vec{B}\xi}{\hbar^2\pi(1-e^{-\delta r})^2}e^{-\delta r}\\-\frac{\left[(m-\gamma)^2-\frac{1}{4}\right]\delta^2}{(1-e^{-\delta r})^2}\end{matrix}\right]\Omega_{nm}(r)=0 \quad (27)$$

where we have defined the following parameters as $\phi_0=\frac{hc}{e}$ and $\gamma=\frac{\xi}{\phi_0}$.

Now introducing the NUFA method of Eq. (3) into Eq. (27) with the following coordinate transformation $z=e^{-\delta r}$. Equation (27) becomes

$$\frac{d^2\Omega_{nm}(r)}{dz^2}+\frac{1}{z}\frac{d\Omega_{nm}(r)}{dz}+\frac{1}{z^2}\left[\begin{matrix}\frac{2\mu E_{nm}}{\hbar^2\delta^2}-\frac{2\mu D_e}{\hbar^2\delta^2}+\frac{4\mu D_er_e}{\hbar^2\delta(1-z)}-\frac{2\mu D_er_e^2}{\hbar^2(1-z)^2}\\+\frac{2\mu C}{\hbar^2\delta(1-z)}z+\frac{2\mu C\tilde{g}E_{nm}}{\hbar^2\delta(1-z)}z+\frac{2m\lambda\vec{B}}{\hbar\delta(1-z)^2}z\\-\frac{\lambda^2\vec{B}^2}{\hbar^2\delta^2(1-z)^2}z^2-\frac{\lambda^2\vec{B}\xi}{\hbar^2\pi\delta(1-z)^2}z-\frac{\left[(m-\gamma)^2-\frac{1}{4}\right]}{(1-z)^2}\end{matrix}\right]\Omega_{nm}(r)=0 \quad (28)$$

To make Eq. (28) solvable with NUFA method, let's introduce the following dimensionless parameters

$$-\varepsilon_{nm}=\frac{2\mu E_{nm}}{\hbar^2\delta^2},Q_1=-\frac{2\mu D_e}{\hbar^2\delta^2},Q_2=\frac{4\mu D_er_e}{\hbar^2\delta},Q_3=-\frac{2\mu D_er_e^2}{\hbar^2},Q_4=\frac{2\mu C}{\hbar^2\delta},Q_5=\frac{2\mu a\tilde{g}E_{nm}}{\hbar^2\delta},Q_6=\frac{2m\lambda\vec{B}}{\hbar\delta},Q_7=-\frac{\lambda^2\vec{B}^2}{\hbar^2\delta^2},$$
$$Q_8=-\frac{\lambda^2\vec{B}\xi}{\hbar^2\delta\pi},Q_9=-\left[(m-\gamma)^2-\frac{1}{4}\right] \quad (29)$$

$$\frac{d^2\Omega_{nm}(r)}{dz^2}+\frac{1}{z}\frac{d\Omega_{nm}(r)}{dz}+\frac{1}{z^2}\left[\begin{matrix}-\varepsilon_{nm}+Q_1+\frac{Q_2}{(1-z)}+\frac{Q_3}{(1-z)^2}+\frac{Q_4z}{(1-z)}+\frac{Q_5z}{(1-z)}\\+\frac{Q_6z}{(1-z)^2}+\frac{Q_7z^2}{(1-z)^2}+\frac{Q_8z}{(1-z)^2}+\frac{Q_9}{(1-z)^2}\end{matrix}\right]\Omega_{nm}(r)=0 \quad (30)$$

and for mathematical simplicity and convenience Eq. (30) becomes:

$$\frac{d^2\Omega_{nm}(r)}{dz^2}+\frac{(1-z)}{z(1-z)}\frac{d\Omega_{nm}(r)}{dz}+\frac{1}{z^2(1-z)^2}[-(\varepsilon_{nm}+p_1)z^2+(2\varepsilon_{nm}+p_2)z-(\varepsilon_{nm}+p_3)]\Omega_{nm}(r)=0 \quad (31)$$

Where

$$p_1=-Q_1+Q_4+Q_5-Q_7,\quad p_2=-2Q_1-Q_2+Q_4+Q_5+Q_6+Q_8,\quad p_3=-Q_1-Q_2-Q_3-Q_9 \quad (32)$$

And

$$\alpha_1=\alpha_2=\alpha_3=1,\ \xi_1=\varepsilon_{nm}+p_1,\ \xi_2=2\varepsilon_{nm}+p_2,\ \xi_3=\varepsilon_{nm}+p_3 \quad (33)$$

By comparing Eq. (31) with the NUFA method of Eq. (3), then we obtain the following:

$$\lambda=\sqrt{\varepsilon_{nm}+p_3} \quad (34)$$

and

$$v=\frac{1}{2}+\sqrt{\frac{1}{4}+\xi_1-\xi_2+\xi_3} \quad (35)$$

Substituting Eqs. (33), (34) and (35) into Eq. (17), we get the energy eigenvalues as:

$$\varepsilon_{nm}+p_3=\left[\frac{p_1-p_3-(n+v)^2}{2(n+v)}\right]^2 \quad (36)$$

Substituting Eqs. (29) and (32) into Eq. (36), we get

$$E_{nm}=D_e-2D_e\delta r_e+D_e\delta^2r_e^2+\frac{\hbar^2\delta^2}{2\mu}\left[(m-\gamma)^2-\frac{1}{4}\right]-\frac{\hbar^2\delta^2}{2\mu}\left[\frac{\frac{2\mu C}{\hbar^2\delta}+\frac{2\mu C\tilde{g}E_{nm}}{\hbar^2\delta}+\frac{\tilde{\lambda}^2\vec{B}^2}{\hbar^2\delta^2}+\frac{4\mu D_er_e}{\hbar^2\delta}-\frac{2\mu D_er_e^2}{\hbar^2}-\left[(m-\gamma)^2-\frac{1}{4}\right]-(n+v)^2}{2(n+v)}\right]^2 \quad (37)$$

where

$$\lambda = \frac{1}{2} + \sqrt{\frac{\tilde{\lambda}^2\vec{B}^2}{\hbar^2\delta^2} + \frac{2\mu D_e r_e^2}{\hbar^2} + (m-\gamma)^2 - \frac{2m\tilde{\lambda}\vec{B}}{\hbar\delta} + \frac{\tilde{\lambda}^2\vec{B}\xi}{\hbar^2\delta\pi}} \tag{38}$$

Equation (37) is an implicit self-consistent equation for the bound-state energy E_{nm}, as it appears on both sides. It is solved numerically using an iterative procedure, starting from an initial guess and updating until convergence is achieved within a specified tolerance. Some optional methods of solution includes fixed-point iteration, Newton–Raphson, or fsolve.

Substituting Eqs. (29), (32) and (33) into Eq. (18), the corresponding Energy eigenfunction equation can be obtained as:

$$\Omega_{nm}(z) = \aleph_{n\ell} z^{\sqrt{-\frac{2\mu E_{nm}}{\hbar^2\delta^2} + \frac{2\mu D_e}{\hbar^2\delta^2} - \frac{4\mu D_e r_e}{\hbar^2\delta} + \frac{2\mu D_e r_e^2}{\hbar^2} + \left[(m-\gamma)^2 - \frac{1}{4}\right]}} \times (1-z)^{\frac{1}{2} + \sqrt{\frac{1}{4} + \frac{2\mu D_e}{\hbar^2\delta^2} + \frac{2\mu C}{\hbar^2\delta} + \frac{2\mu C\tilde{g}E_{nm}}{\hbar^2\delta} + \frac{\lambda^2\vec{B}^2}{\hbar^2\delta^2}}} {}_2F_1(a,b,c;z) \tag{39}$$

where $a = \beta + \sigma + \sqrt{\varepsilon_{nm} + p_1}$, $b = \beta + \sigma - \sqrt{\varepsilon_{nm} + p_1}$, $c = 1 + 2\beta$ and $\aleph_{n\ell}$ is the normalization constant.

Magnetic Properties of TiH Diatomic Molecule

It is well known that the partition function of a system can be used to obtain all thermodynamic and magnetic properties (Edet *et al*, 2022). Easy summation over all vibrational energy levels available to the system can be used to calculate the vibrational partition function. Given the energy spectrum in Eq. (37), the partition function $Z(\beta)$ of the titanium hydride with Modified Kratzer potential Energy-Dependent Screened Coulomb potential at finite temperature, T, is obtained with the Boltzmann factor as;

$$Z(\beta) = \sum_{n=0}^{n_{max}\Sigma} e^{-\beta E_n} \tag{40}$$

where $\beta = \frac{1}{k_\beta T}$, k_B is the Boltzmann's constant. To calculate the summation in the partition function, the energy eigenvalues in Eq. (39) can be rewritten in the compact form;

$$E_{nm} = P_1 - \frac{\hbar^2\alpha^2}{2\mu}\left(\frac{R_1 - (n+v)^2}{2(n+v)}\right)^2 \tag{41}$$

where

$$P_1 = D_e - 2D_e\delta r_e + D_e\delta^2 r_e^2 + \frac{\hbar^2\delta^2}{2\mu}\left[(m-\gamma)^2 - \frac{1}{4}\right] \tag{42}$$

$$R_1 = \frac{2\mu C}{\hbar^2\delta} + \frac{2\mu C\tilde{g}E_{nm}}{\hbar^2\delta} + \frac{\lambda^2\vec{B}^2}{\hbar^2\delta^2} + \frac{4\mu D_e r_e}{\hbar^2\delta} - \frac{2\mu D_e r_e^2}{\hbar^2} - \left[(m-\gamma)^2 - \frac{1}{4}\right] \tag{43}$$

$$v = \frac{1}{2} + \sqrt{\frac{\lambda^2\vec{B}^2}{\hbar^2\delta^2} + \frac{2\mu D_e r_e^2}{\hbar^2} + (m-\gamma)^2 - \frac{2m\lambda\vec{B}}{\hbar\delta} + \frac{\lambda^2\vec{B}\xi}{\hbar^2\delta\pi}} \tag{44}$$

It should be noted here that the maximum value n_{max}can be obtained by setting $\frac{dE_n}{dn=0}$.

$$n\sqrt{P_1}_{max} \tag{45}$$

To evaluate the integral in Eq. (40), we write the integral as follows:

$$Z(\beta) = \int_0^{n_{max}\int} e^{\beta\left(P_2(n+v)^2 + \frac{Q}{(n+v)} + R_2\right)} \tag{46}$$

or explicitly

$$Z(\beta) = \int_v^{n_{max}\int} e^{\beta\left(P_2\rho^2 + \frac{Q}{\rho^2} + R_2\right)} \tag{47}$$

where we have defined; $\rho = n + v$, $P_2 = \frac{\hbar^2\alpha^2}{8\mu}$, $Q = \frac{\hbar^2\alpha^2 R_1^2}{8\mu}$, $R_2 = \frac{\hbar^2\alpha^2 R_1}{4\mu} - P_1$ and the limits of integral is given as: $v \leq \rho \leq n_{max}$

Evaluating Eq. (47), the partition function of the titanium hydride with modified Kratzer potential plus Energy-Dependent screened Coulomb potential in the presence of magnetic and AB-flux fields is obtain as follows using Mathematica 9.0 Software;

$$Z(\beta) = -\frac{e^{-2\sqrt{-Q\beta}\sqrt{-\beta P_2} + \beta R_2}\sqrt{\pi}\left(-Erf[\Xi_1] + \Delta_3 Erf[\Xi_2] + Erf[\Xi_3] - \Delta_3 Erf[\Xi_4]\right)}{4\sqrt{-\beta P_2}} \tag{48}$$

where we have used the following notations for mathematical simplicity and convenience

$$\Xi_1 = \frac{\sqrt{-Q\beta}}{v} - v\sqrt{-\beta P_2},\ \Xi_2 = \frac{\sqrt{-Q\beta}}{v} + v\sqrt{-\beta P_2},\ \Xi_3 = \frac{\sqrt{-Q\beta}}{v} - v\sqrt{-\beta P_2} - n\sqrt{-\beta P_2},\ \Xi_4 = \frac{\sqrt{-Q\beta}}{v} + v\sqrt{-\beta P_2} + n\sqrt{-\beta P_2} \text{ and } \Delta_3 = e^{4\sqrt{-Q\beta}\sqrt{-\beta P_2}} \tag{49}$$

where Erf denotes the error function which can be defined as

$$Erf(z) = \frac{2}{\sqrt{\pi}}\int_0^z e^{t^2}\,dt \qquad (50)$$

The partition function in Eq. (40) can be used to obtain magnetic properties of the Modified Kratzer potential plus Energy-Dependent Screened Coulomb potential in the presence of the magnetic and AB-flux fields, such as the magnetization (M), magnetic susceptibility (χ_m), and persistent current (I). The following expressions can be used to calculate the system's magnetic properties (Edet *et al*, 2022):

$$M(\beta) = \frac{1}{\beta}\left(\frac{1}{Z(\beta)}\right)\left(\frac{\partial}{\partial \vec{B}}Z(\beta)\right) \qquad (51)$$

$$\chi_m(\beta) = \frac{\partial M(\beta)}{\partial \vec{B}} \qquad (52)$$

and

$$I(\beta) = -\frac{e}{hc}\frac{\partial F(\beta)}{\partial m} \qquad (53)$$

RESULTS AND DISCUSSION

The obtained energy eigenvalues results are discussed graphically in this section, focusing on the magnetic properties of the titanium hydride diatomic molecule. For all calculations, the molecular and physical parameters are chosen as

$D_e = 2.05$ eV, $r_e = 1.781$ Å, $\delta = 1.32408$ Å^{-1}, $\mu = 0.987371$ a.m.u $= 931.494028$ MeVc^{-2}, $\hbar c = 1973.269$ eVÅ Oyewumi *et al.*, 2014).

Magnetic Properties Versus Inverse Temperature

Figure 1 illustrates the variation of the partition function with inverse temperature for slope parameter values $\tilde{g} = -1, 0, +1$. Each curve starts from a distinct value in the negative domain and increases monotonically with increasing inverse temperature. At higher inverse temperature values, all curves exhibit convergent behavior toward a common value. The curve corresponding to $\tilde{g} = -1$ lies above those for $\tilde{g} = 0$and $\tilde{g} = +1$, with the separation between the curves gradually narrowing as convergence occurs.

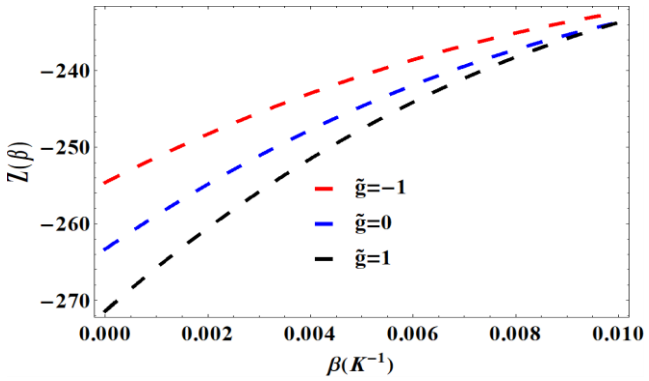

Figure 1: Partition function as a function of inverse temperature $\beta(K^{-1})$varying with Energy slope parameter $\tilde{g}$

Figure 2 below shows the variation of magnetization with inverse temperature. Magnetization decreases monotonically with increasing inverse temperature for all slope parameter values, remaining entirely in the positive domain. The curve for $\tilde{g} = -1$lies innermost, followed by $\tilde{g} = 0$, and then $\tilde{g} = +1$. The nearly constant spacing between the curves indicates uniform relative behavior across slope values.

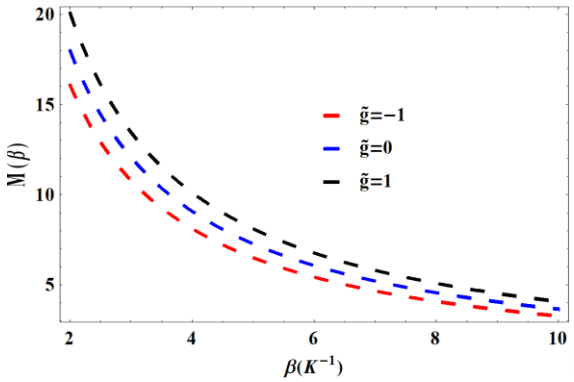

Figure 2: Magnetization as a function of inverse temperature $\beta(K^{-1})$varying with Energy slope parameter $\tilde{g}$

Figure 3 below presents the magnetic susceptibility as a function of inverse temperature. All curves lie in the negative susceptibility domain and increase monotonically with increasing inverse temperature, approaching a common convergence point. The curve for $\tilde{g} = -1$ is outermost, followed by $\tilde{g} = 0$ and $\tilde{g} = +1$. Although initially distinct, the spacing between the curves decreases at higher inverse temperatures.

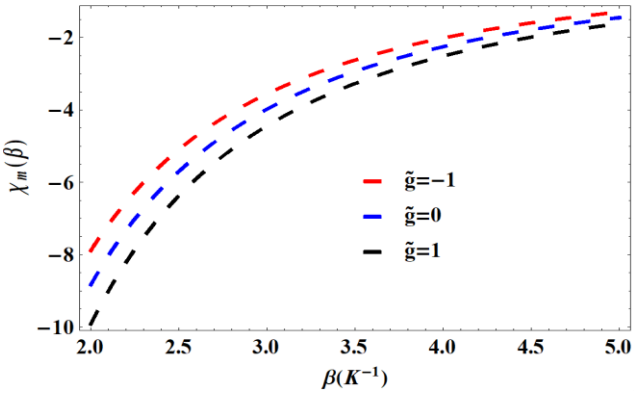

Figure 3: Magnetic Susceptibility as a function of inverse temperature $\beta(K^{-1})$varying with Energy slope parameter $\tilde{g}$

Figure 4 below depicts the variation of persistent current with inverse temperature. Persistent current decreases monotonically with increasing inverse temperature and remains in the positive domain. The curve for $\tilde{g} = -1$has the lowest magnitude, $\tilde{g} = 0$lies intermediate, and $\tilde{g} = +1$ produces the highest persistent current values.

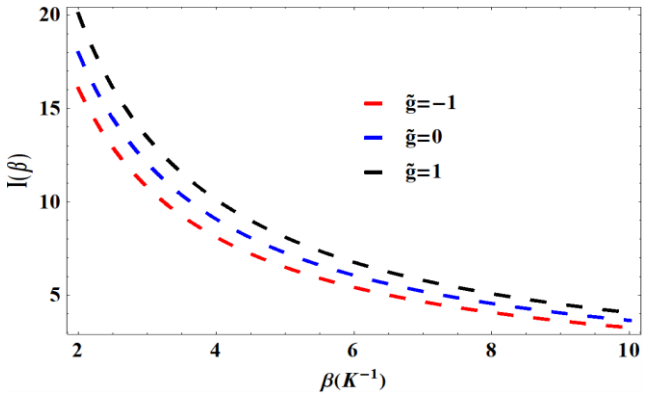

Figure 4: Persistent current as a function of inverse temperature $\beta(K^{-1})$varying with Energy slope parameter $\tilde{g}$

Magnetic Properties Versus Magnetic Field

Figure 5 shows the partition function as a function of magnetic field for the three slope parameter values. All curves begin with saturation at zero and undergo a sharp drop around magnetic field values of approximately 0.0008–0.0009 T. Beyond this region, the curves diverge slightly while maintaining consistent relative positions. The outermost curve corresponds to $\tilde{g} = -1$, followed by $\tilde{g} = 0$, with $\tilde{g} = +1$innermost.

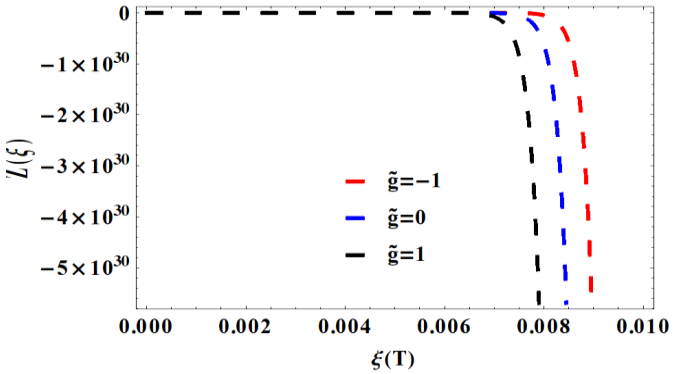

Figure 5: Partition function as a function of AB-flux field $\xi(T)$varying with Energy slope parameter $\tilde{g}$

Figure 6 below illustrates the variation of magnetization with magnetic field. Magnetization increases with increasing magnetic field and remains positive for all slope values. The curve for $\tilde{g} = -1$crosses that of $\tilde{g} = 0$at very low magnetic fields $(B < 0.0002\ \mathrm{T})$ before diverging more strongly. The curves for $\tilde{g} = 0$and $\tilde{g} = +1$remain closely spaced, with $\tilde{g} = +1$producing the highest magnetization values.

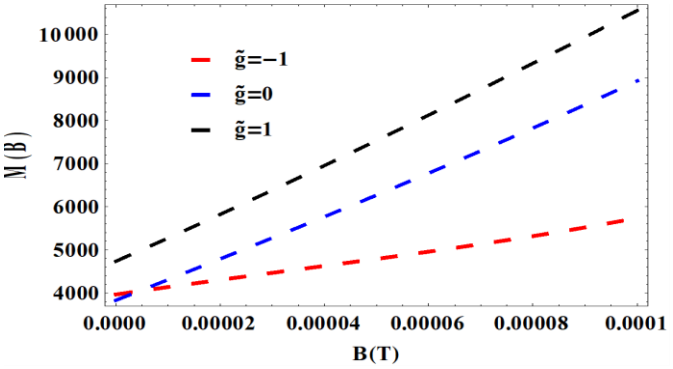

Figure 6: Magnetization as a function of magnetic field $B(T)$varying with Energy slope parameter $\tilde{g}$

Figure 7 below presents magnetic susceptibility as a function of magnetic field. All curves lie in the positive domain. The $\tilde{g} = -1$ curve exhibits non-monotonic behavior, showing an initial decrease followed by an increase. The $\tilde{g} = 0$curve increases smoothly, while $\tilde{g} = +1$rises more rapidly toward early saturation.

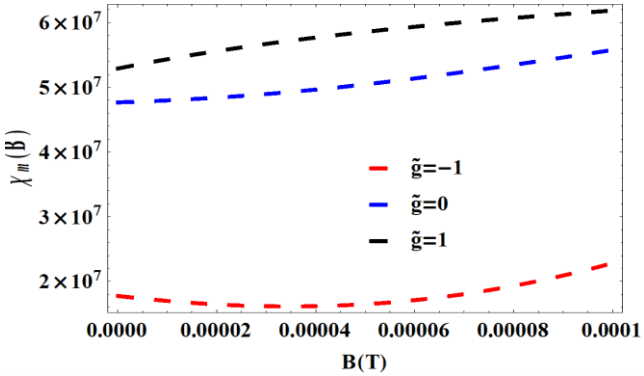

Figure 7: Magnetic Susceptibility as a function of magnetic field $B(T)$varying with Energy slope parameter $\tilde{g}$

Figure 8 below shows the persistent current versus magnetic field. The curves diverge increasingly with magnetic field strength. The curve for $\tilde{g} = +1$is uppermost, followed by $\tilde{g} = 0$, while $\tilde{g} = -1$lies lowest after crossing the $\tilde{g} = 0$curve at low magnetic field values.

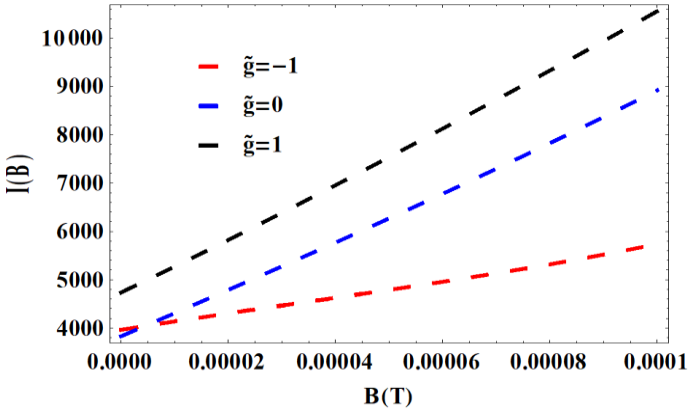

Figure 8: Persistent current as a function of magnetic field $B(T)$varying with Energy slope parameter $\tilde{g}$

Magnetic Properties Versus Aharonov–Bohm Flux Field

Figure 9 displays the partition function as a function of the AB-flux field. All curves initially saturate at zero and then experience a sharp decline around 0.008–0.009 T. After this drop, the curve for $\tilde{g} = -1$lies outermost, followed by $\tilde{g} = 0$ and $\tilde{g} = +1$. The spacing between curves remains nearly constant thereafter.

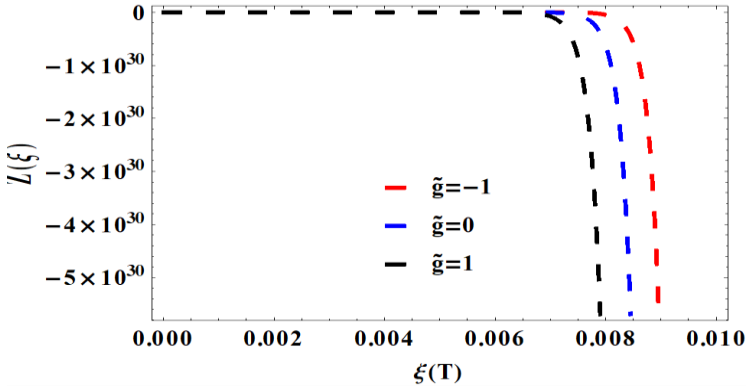

Figure 9: Partition function as a function of AB-flux field $\xi(T)$varying with Energy slope parameter $\tilde{g}$

Figure 10 below shows the magnetization versus AB-flux field. All curves exhibit an initial sharp drop to a minimum at AB-flux values below 0.002 T, followed by a rapid increase and eventual saturation near 4750 units. After the minima, the curve for $\tilde{g} = -1$is uppermost, followed by $\tilde{g} = 0$, with $\tilde{g} = +1$ lowest.

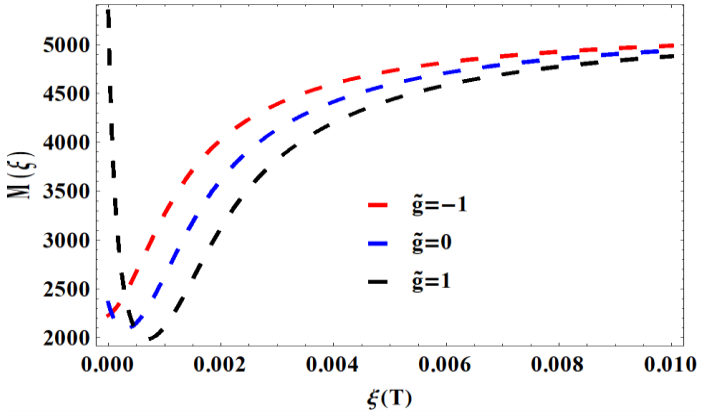

Figure 10: Magnetization as a function of AB-flux field $\xi(T)$varying with Energy slope parameter $\tilde{g}$

Figure 11 belwo presents the magnetic susceptibility versus AB-flux field. All curves lie in the negative domain. The susceptibility for $\tilde{g} = -1$remains constant at zero, while $\tilde{g} = 0$shows a nearly flat negative response. In contrast, $\tilde{g} = +1$exhibits a large negative susceptibility at low flux values, followed by a rapid increase and eventual convergence with the other curves.

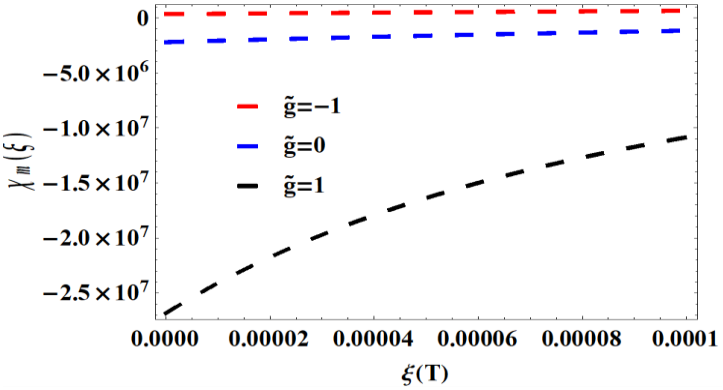

Figure 11: Magnetic Susceptibility as a function of AB-flux field $\xi(T)$varying with Energy slope parameter $\tilde{g}$

Figure 12 below depicts the persistent current versus AB-flux field. All curves show a sharp rise around 0.01 T, followed by saturation and convergence near 5150 units. The persistent current is highest for $\tilde{g} = -1$, intermediate for $\tilde{g} = 0$, and lowest for $\tilde{g} = +1$.

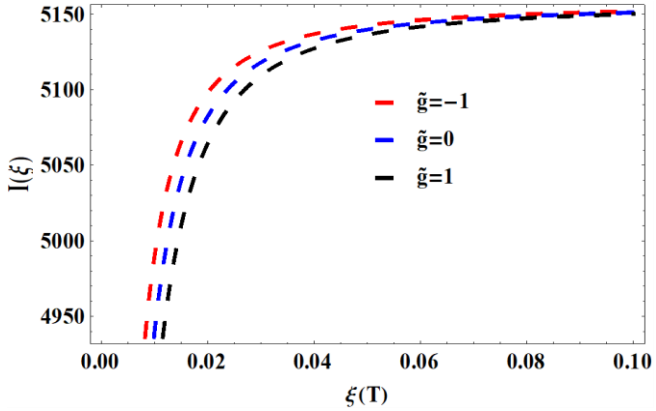

Figure 12: Persistent current as a function of AB-flux field $\xi(T)$varying with Energy slope parameter $\tilde{g}$

CONCLUSION

In this work, the magnetic properties of the titanium hydride diatomic molecule have been investigated using the modified Kratzer energy-dependent screened Coulomb potential in the presence of external magnetic and Aharonov–Bohm flux fields. Closed-form solutions of the Schrödinger equation were obtained via the Nikiforov–Uvarov Functional Analysis method and used to evaluate thermodynamic and magnetic quantities. The results show that the slope parameter plays a decisive role in determining the strength, ordering, and convergence behavior of the partition function, magnetization, magnetic susceptibility, and persistent current. Negative slope values enhance magnetic responses, while positive values suppress them. External magnetic fields induce divergence and saturation effects, whereas AB-flux fields produce sharp transitions, minima, and convergence phenomena. Overall, the combined influence of the slope parameter and external fields provides an effective mechanism for tuning the magnetic behavior of the TiH diatomic molecule, with potential relevance to molecular magnetism, spectroscopy, and field-controlled quantum systems.

REFERENCES

Abu-Shady, M., Abdel-Karim, T. A., & Khokha, E. M. (2021). Non-relativistic quark model under external magnetic and Aharonov–Bohm (AB) fields in the presence of temperature-dependent confined Cornell potential. *Canadian Journal of Physics*, 99, 1–8. https://doi.org/10.1139/cjp-2020-0101

Dong, S. H., & Cruz-Irisson, M. (2012). Energy spectrum for a modified Rosen–Morse potential solved by proper quantization rule and its thermodynamic properties. *Journal of Mathematical Chemistry, 50*, 881–892. https://doi.org/10.1007/s10910-011-9931-3

Ebeling, W., & Sokolov, I. (2005). *Statistical thermodynamics and stochastic theory of nonequilibrium systems*. World Scientific.

Edet, C. O., Khordad, R., Ettah, E. B., Aljunid, S. A., Endut, R., Ali, N., Asjad, M., Ushie, P. O., & Ikot, A. N. (2022). Magneto-transport and thermal properties of TiH diatomic molecule under the influence of magnetic and Aharonov–Bohm (AB) fields. *Scientific Reports, 12*, 15430. https://doi.org/10.1038/s41598-022-19396-x

Edet, C.O., Ikot, A.N., Okorie, U.S. Rampho, G. J., Ramantswana, M., Horchani, R., Abdullah, H., Vinasco, J. A., Duque, C. A. & Abdel-Haleem Abdel-Aty (2021). Persistent Current, Magnetic Susceptibility, and Thermal Properties for a Class of Yukawa Potential in the Presence of External Magnetic and Aharanov–Bohm Fields. *Int J Thermophys* 42, 138. https://doi.org/10.1007/s10765-021-02891-0

Eshghi, M., & Mehraban, H. (2017). Study of a 2D charged particle confined by magnetic and Aharonov–Bohm flux fields under the radial scalar power potential. *European Physical Journal Plus, 132*(3), 121. https://doi.org/10.1140/epjp/i2017-11379-x

Greene, R. L., & Aldrich, C. (1976). Variational wave functions for a screened Coulomb potential. *Physical Review A, 14*, 2363–2366. https://doi.org/10.1103/PhysRevA.14.2363

Gumber, S., Kumar, M., Gambhir, M., Mohan, M., & Kumar, P. (2015). Thermal and magnetic properties of cylindrical quantum dot with asymmetric confinement. *Canadian Journal of Physics, 93*(11), 1264–1268. https://doi.org/10.1139/cjp-2014-0688

Ikot, A. N., Edet, C. O., Amadi, P. O., Okorie, U. S., Rampho, G. J. & Abdullah, H. Y. (2020). Thermodynamic Properties of Aharonov-Bohm and Magnetic Fields with Screened Kratzer Potential. *European Physical Journal* D, 74:159, 1-13. https://doi.org/10.1140/epjd/e2020-10084-9

Ikot, A. N., Azogor, W., Okorie, U. S., Bazauye, F. E., Onjeaju, M. C., Onate, C. A. & Chukwuocha, E. O. (2019). Exact and Poisson summation thermodynamic properties for diatomic molecules with Tietz potential. *Indian Journal of Physics,* 93, 1171–1179. https://doi.org/10.1007/s12648-019-01375-0

Ikot, A. N., Okorie, U. S., Sever, R., & Rampho, G. J. (2019). Eigensolutions, expectation values and thermodynamic properties of the screened-Kratzer potential. *European Physical Journal Plus, 134*, 386. https://doi.org/10.1140/epjp/i2019-12783-x

Ikot, A. N., Okorie, U. S., Osobonye, G., Amadi, P. O., Edet, C. O., Sithole, M. J., Rampho, G. J., & Sever, R. (2020). Superstatistics of Schrödinger equation with pseudo-harmonic potential in external magnetic and Aharonov–Bohm fields. *Heliyon, 6*, e03738. https://doi.org/10.1016/j.heliyon.2020.e03738

Ikot, A. N., Okorie, U. S., Amadi, P. O., Edet, C. O., Rampho, G. J., & Sever, R. (2021). The Nikiforov–Uvarov functional analysis method: A new approach for solving exponential-type potentials. *Few-Body Systems, 62*, 9. https://doi.org/10.1007/s00601-021-01593-5

Oyewumi, K. J., Falaye, B. J., Onate, C. A., Oluwadare, O. J., & Yahaya, W. A. (2014). Thermodynamic

properties and approximate solutions of the Schrödinger equation with the shifted Deng–Fan potential model. *Molecular Physics, 112*, 127–141. https://doi.org/10.1080/00268976.2013.804960

Onate, C. A., & Onyeaju, M. C. (2016). Dirac particles in the field of Frost–Musulin diatomic potential and thermodynamic properties via parametric Nikiforov–Uvarov method. *Sri Lanka Journal of Physics, 17*, 1–17. https://doi.org/10.4038/sljp.v17i0.8027

Purohit, K. R., Parmar, R. H., & Rai, A. K. (2020). Bound state solution and thermodynamical properties of the screened cosine Kratzer potential under the influence of magnetic and Aharonov–Bohm flux fields. *Annals of Physics*, 168335. https://doi.org/10.1016/j.aop.2020.168335

Rampho, G. J., Ikot, A. N., Edet, C. O., & Okorie, U. S. (2020). Energy spectra and thermal properties of diatomic molecules in the presence of magnetic and AB fields with improved
Kratzer potential. *Molecular Physics*, e1821922. https://doi.org/10.1080/00268976.2020.1821922

Song, X. Q., Wang, C. W., & Jia, C. S. (2017). Thermodynamic properties for the sodium dimer. *Chemical Physics Letters, 673*, 50–55. https://doi.org/10.1016/j.cplett.2017.02.010

Sever, R., Tezcan, C., Yesiltas, Ö., & Bucurgat, M. (2008). Exact solution of effective mass Schrödinger equation for the Hulthén potential. International Journal of Theoretical Physics, 47(9), 2243–2248. https://doi.org/10.1007/s10773-008-9656-7

Tezcan, C. & Sever, R. (2009). A general approach for the exact solution of the Schrödinger Equation. *International Journal of Theoretical Physics*, 48(2), 337-350. https://doi.org/10.1007/s10910-007-9233-y